

Ferroelectric and dielectric properties of Ca²⁺-doped and Ca²⁺-Ti⁴⁺ co-doped K_{0.5}Na_{0.5}NbO₃ thin films

Nikolai Helth Gaukås^a, Julia Glaum^a, Mari-Ann Einarsrud^a and Tor Grande^{a*}

Received 00th January 20xx,
Accepted 00th January 20xx

DOI: 10.1039/x0xx00000x

Chemical solution deposition (CSD) of K_{0.5}Na_{0.5}NbO₃ (KNN) thin films on silicon-based substrates is an interesting technology for fabrication of lead-free ferroelectric thin films. Here, we report on improved ferroelectric and dielectric properties of KNN thin films prepared by CSD through Ca²⁺-doping and Ca²⁺-Ti⁴⁺ (CaTiO₃) co-doping. Undoped KNN, 0.5 mol% Ca²⁺-doped and 0.5 mol% CaTiO₃-doped KNN films were deposited on platinized silicon substrates by aqueous CSD. X-ray diffraction of the films as well as powders, prepared from the precursor solutions, confirmed that the three KNN materials were single phase solid solutions. A smaller grain size was observed for the doped relative to undoped KNN films. In contrast to the pure KNN films, the Ca²⁺- and CaTiO₃-doping was observed to promote ferroelectric switching, with a low leakage current and remnant polarization of 6.37±0.47 and 7.40±0.09 μC cm⁻² of the Ca²⁺- and CaTiO₃-doped films, respectively. The dielectric constants of the films were among the highest measured for KNN films from CSD and span from 1800 to 3200 at 1 kHz.

Introduction

Potassium sodium niobate-based (K_{0.5}Na_{0.5}NbO₃, KNN) piezoelectric ceramics have received considerable attention as an environmentally friendly alternative to lead zirconate titanate-based materials (PbZr_xTi_{1-x}O₃, PZT)^{1–4}. Lead-free, non-toxic and biocompatible alternatives to PZT are especially important for *in vivo* biomedical applications⁵, and KNN has shown promising results in biocompatibility tests^{6–13}. Materials in form of thin films are desired in many of these applications and there has been a considerable focus on development of KNN thin films^{14–16}. To bring lead-free piezoelectric ceramics to the marked, economically viable large-scale industrial fabrication routes are required². Chemical solution deposition (CSD) is a cheap and reliable synthesis technique capable of high-volume production of oxide thin films¹⁷. Synthesis of KNN thin films via CSD is usually performed using niobium ethoxide and alkali ethoxides or acetates as precursors, and 2-methoxyethanol as the solvent^{18–49}. In only a few studies other solvents have been used, e.g. propionic acid⁵⁰, ethanol⁵¹, water^{52–57} and other^{58,59}. Due to low cost and the ubiquity of Si in electronics, platinized silicon (SiPt, Pt/TiO₂/SiO₂/Si) is by far the most used substrate in ferroelectric oxide thin film CSD synthesis¹⁷. KNN thin film synthesis is no exception, and the majority of studies of KNN thin films are based on using SiPt substrates^{19–24,28–36,40–43,46–48,52,53}, while a few other studies are reported using other substrates like SiO₂/Si^{38,58,59}, ZrO₂/Si^{44,45}, LaNiO₃/Si⁵⁷, Pt/MgO³⁹, Pt/Al₂O₃^{49,58}, metals^{50,51,54} and SrTiO₃ (STO)^{18,25–27,37,55,56}.

Compositional engineering is readily used to improve the functional properties of bulk KNN ceramics^{1,4}. Compositional engineering is typically applied to reduce the leakage current in KNN thin films by doping with Mn²⁺^{18–20,25,28–30,34,36,37,42,43,48} or Co²⁺^{35,36}, or to improve the ferroelectric properties by altering phase boundaries using Li⁺^{22,27,28,31,32}, Ta⁵⁺^{19,21}, Li⁺ and Ta⁵⁺^{20,34} or Li⁺, Ta⁵⁺ and Sb⁵⁺³³. Except for Ta⁵⁺, these dopants are toxic, and alternative dopants are required when developing KNN-based ceramics for certain technologies, e.g. *in vivo* biomedical applications⁶⁰. Ca²⁺ and Ti⁴⁺ are both non-toxic, and therefore suitable for *in vivo* applications^{61,62}. Ca²⁺ doping is reported to have a softening effect on the ferroelectric properties of bulk KNN⁶³, improve dielectric properties⁶⁴ and to increase the piezoelectric coefficient (*d*₃₃ or *d*₃₃^{*}) compared to undoped KNN^{63–66}. Enhanced ferroelectric performance has been reported for bulk KNN doped with 0.55, 1 and 5 mol% CaTiO₃^{67–71}. These dopants have also been reported to increase the densification^{65–67,70} and to reduce ion-release from KNN in aqueous media⁶⁶. Finally, Ikeuchi et al.⁷² demonstrated improved piezoelectric properties in RF magnetron sputtered KNN films doped with 0–6.5 mol% CaTiO₃.

Here, we report on improved ferroelectric and dielectric properties of KNN thin films doped with Ca²⁺ and co-doping with stoichiometric amount of Ca²⁺ and Ti⁴⁺ corresponding to CaTiO₃. KNN films doped with 0.5 mol% Ca²⁺ and 0.5 mol% CaTiO₃ were prepared on SiPt substrates by aqueous CSD, previously applied to fabricate KNN thin films on STO substrates⁵⁶. Powders were also prepared from the same solutions to provide information concerning crystal structure and coarsening during thermal annealing. We demonstrate that this doping of the KNN films significantly improves the ferroelectric properties, which is discussed in relation to microstructure, dielectric properties and possible point defects in the doped KNN materials.

^a Department of Materials Science and Engineering, Norwegian University of Science and Technology (NTNU), N-7491 Trondheim, Norway.

*Corresponding author. E-mail: grande@ntnu.no

Electronic Supplementary Information (ESI) available: [details of any supplementary information available should be included here]. See DOI: 10.1039/x0xx00000x

Experimental

Materials synthesis

Precursor solutions for the materials with the acronyms KNN, KNN-Ca²⁺ and KNN-CaTiO₃, summarized in Table 1, were prepared using an aqueous malic acid-complexed niobium solution as described previously⁵⁶. The niobium solution was prepared by first precipitating niobic acid by adding an ammonia solution (25 wt%, VWR Chemicals, Radnor, PA, USA) to an aqueous solution of NH₄NbO(C₂O₄)₂·xH₂O (99.99%, Sigma-Aldrich, St. Louis, MO, USA). The niobic acid precipitate was dissolved in a solution of deionized water and DL-malic acid (99%, Sigma-Aldrich) with a molar ratio corresponding to 1:2 (Nb:malic acid). Pre-dried NaNO₃ (99%, Sigma-Aldrich) and KNO₃ (99%, Alfa Aesar, Haverhill, MA, USA) were dissolved in the niobium solution, and the pH was adjusted to ~7 using ammonia solution. 5 mol% excess of Na⁺ and K⁺ was used in all the solutions, and the concentration of the Nb in the final solutions was ~0.09 M. The KNN-Ca²⁺ and KNN-CaTiO₃ precursor solutions were prepared by adding solutions of Ca²⁺ and Ti⁴⁺ to the KNN solution. Ca(NO₃)₂·4H₂O (99%, Sigma Aldrich) was dissolved in deionized water using ethylenediaminetetraacetic acid (EDTA, 99%, Sigma Aldrich) as complexing agent in the ratio of 1:2 (Ca²⁺:EDTA). The pH was adjusted to 8 using ammonia solution, and the final concentration of the Ca²⁺-solution was 3.23·10⁻² M. Ti-4-isopropoxide (97%, Sigma-Aldrich) was dissolved in deionized water at 80 °C using citric acid (CA, 99%, Sigma Aldrich) as complexing agent with a ratio of 1:3 (Ti⁴⁺:CA). The pH was adjusted to 8 using ammonia solution, and the final concentration of the Ti⁴⁺-solution was determined by thermogravimetric analysis to be 7.52·10⁻¹ M.

The solutions were deposited on platinized silicon (SiPt, Pt(111)/TiO₂/SiO₂/Si(100), SINTEF MiNaLab, Oslo, Norway) substrates. Prior to the deposition, the substrates were activated in an oxygen plasma cleaner (Femto, Diener Electronics, Ebhausen, Germany) to increase the wettability. The deposition by spin coating was performed using a spin coater (WS-400A-6NPP/C-1, Laurell Technologies, Montgomery, PA, USA), operating at 3500 rpm for 40 s. The deposited films were dried on a hotplate at 200 °C for 3 min and pyrolyzed on a rapid heating plate (described in ⁵⁶) at 550 °C for 5 min using a heating rate of 100 °C min⁻¹. The deposition and heat treatment were repeated 15 and 30 times. The films were

post-annealed at 700 °C for 10 min using a heating rate of 100 °C min⁻¹.

KNN powders were prepared by drying the precursor solutions at 160 °C for 8 h. The dried precursor solutions were calcined and coarsened in air at 700 and 850 °C, respectively, for 4 h (LT 15/12/P330, Nabertherm, Lilienthal, Germany).

Characterization

X-ray diffraction (XRD) patterns of the powders were recorded using Cu K α radiation (D8 Advance, Bruker, Billerica, MA, USA). Grating incidence X-ray diffraction (GIXRD, D8 Advance, Bruker) of the films were recorded using Cu K α radiation and a 2° incidence angle, while conventional Bragg-Brentano XRD of the films were measured using monochromatic Cu K α radiation (D5005, Siemens, Karlsruhe, Germany). Scanning electron microscopy (SEM, Ultra 55, Carl Zeiss AG, Oberkochen, Germany) of the thin films was performed using an in-lens detector and acceleration voltage of 10 kV. For electric characterization of the films, Pt top electrodes (thickness 100 nm) with diameters of 0.5 and 1.0 mm, were deposited by e-beam evaporation (Custom ATC-2200V, AJA International Inc., Scituate, MA, USA) through a shadow mask. Prior to the measurements, the films with the electrodes were heat treated at 400 °C for 2.5 h in flowing oxygen (AccuThermo AW-610, Allwin21, Morgan Hill, CA, USA). Film polarization and capacitance as a function of electric field at room temperature were analyzed with a piezoelectric evaluation system (aixACCT, Aachen, Germany). Relative permittivity as a function of temperature and frequency was studied using AC impedance spectroscopy (Alpha-A High Performance Frequency Analyzer, Novocontrol Technologies, Montabaur, Germany) with a rapid heating plate as temperature controller⁵⁶.

Table 1: Overview of the chemical compositions and acronyms of the KNN-based thin films prepared in this work.

Acronym	Chemical formula	Doping
KNN	(K _{0.5} Na _{0.5})NbO ₃	-
KNN-Ca ²⁺	(K _{0.495} Na _{0.495} Ca _{0.005})NbO ₃	0.5 mol% Ca ²⁺
KNN-CaTiO ₃	(K _{0.4975} Na _{0.4975} Ca _{0.005})Nb _{0.995} Ti _{0.005} O ₃	0.5 mol% Ca ²⁺ and 0.5 mol% Ti ⁴⁺

Results

The powders calcined at 700 and 850 °C were phase pure based on the diffraction patterns shown in Figure 1. All the Bragg reflections can be assigned to monoclinic KNN, and Pawley fits of the diffraction patterns are summarized in Table S.1 in Electronic Supplementary Information (ESI). A coarsening was observed for the powders going from 700 to 850 °C especially for undoped KNN (Table S.1), while no major changes in the unit cell parameters were observed by increasing the calcination temperature. A minor contraction of the unit cell volume and the *c* lattice parameter, and an increase in β -distortion of the unit cell, was observed due to the doping (Table S.1), but no apparent change in symmetry by doping can be inferred from the diffraction patterns.

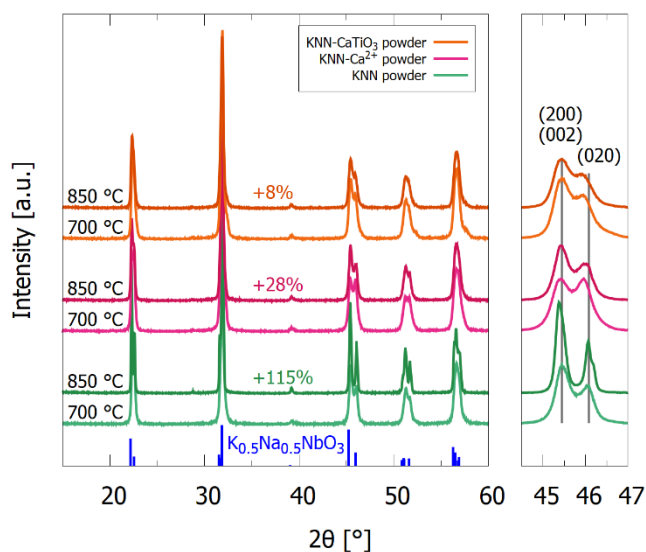


Figure 1: XRD patterns of powders from precursor solutions calcined at 700 and 850 °C, respectively, for 4 h. Percent increase in crystallite size from 700 to 850 °C is marked in the figure above each composition. Reference pattern for $K_{0.5}Na_{0.5}NbO_3$ (blue, PDF card 00-061-0315⁷³) is included.

Electron micrographs of cross sections and the top surfaces of the three different KNN films are shown in Figure 2. Dense and uniform films were successfully deposited on the SiPt substrates. An average thickness of ~ 11 nm per deposition was inferred from the SEM images. The top surface of the films (insets Figure 2) demonstrate coarser grains in the undoped KNN film (~ 85 nm) compared to the films doped with Ca^{2+} and $CaTiO_3$ (~ 70 and ~ 60 nm respectively). No evidence for columnar growth was observed in the cross sections, in agreement with the polycrystalline nature of the films as discussed below.

GIXRD patterns of the films after pyrolysis (550 °C) and annealing (700 °C) presented in Figure 3 show only reflections indexed to KNN and the films appeared phase pure and polycrystalline. The low degree of texture and polycrystalline nature of the films was confirmed by conventional XRD for the undoped KNN film, shown in Figure S.3.

The ferroelectric behaviour of the films was analysed by measuring polarization as a function of electric field.

Polarization-electric field loops measured using a frequency of 10 Hz and an electric field bias of 100 kV cm^{-1} are given in Figure 4. Ferroelectric polarization switching is observed for the doped films (KNN- Ca^{2+} , KNN- $CaTiO_3$), demonstrated by the onset of polarization saturation at increasing field and switching current spikes in the current flux shown in the inset in Figure 4. Ferroelectric polarization switching was not observed for the undoped KNN film, irrespectable of the frequency and field applied.

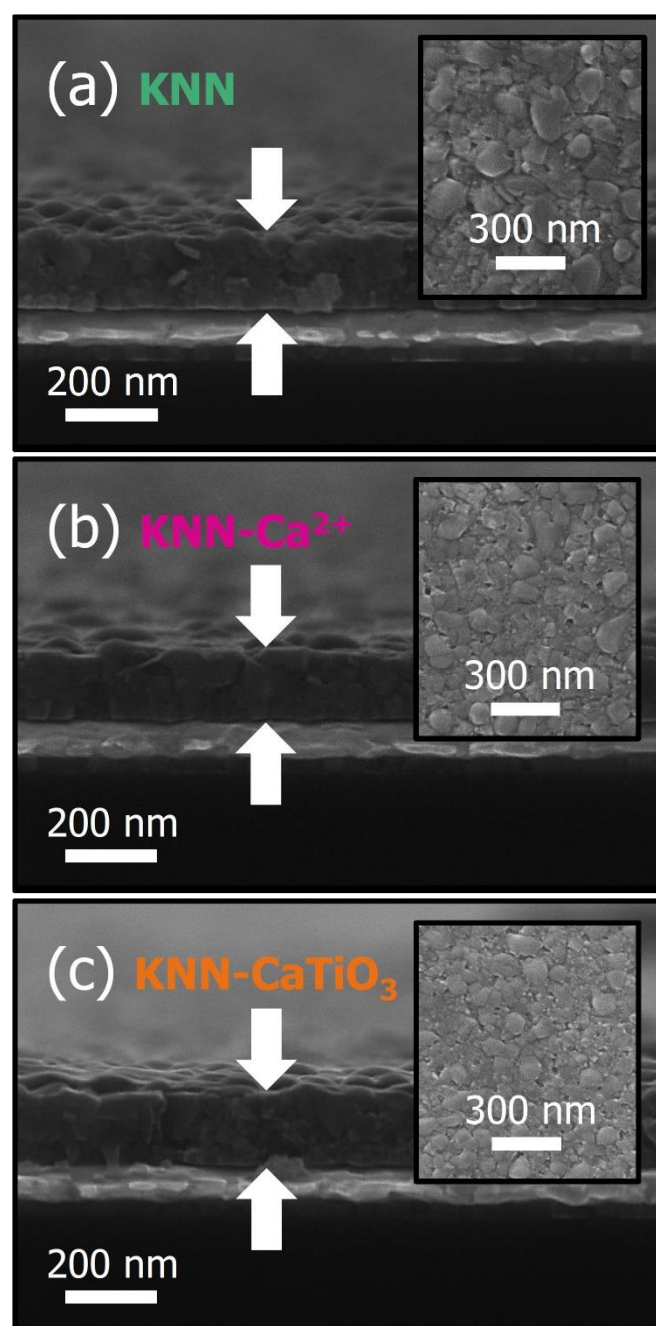


Figure 2: Cross section and top-view SEM micrographs of KNN films prepared by 15 layers. (a) undoped (KNN), (b) 0.5 mol% Ca^{2+} doped (KNN- Ca^{2+}) and (c) 0.5 mol% $CaTiO_3$ doped (KNN- $CaTiO_3$).

The frequency dependency of polarization-electric field hysteresis loops of the doped KNN films between 50 and 5000 Hz is presented in Figure 5. Electric field biases of 125 and 142 kV cm^{-1} were used for the KNN- Ca^{2+} and KNN- CaTiO_3 films, respectively. A decrease in polarization is observed with increasing frequency. The remnant polarization (P_r) at 50 and 1000 Hz is 6.37 ± 0.47 and 4.67 ± 0.04 $\mu\text{C cm}^{-2}$ for the KNN- Ca^{2+} film and 7.40 ± 0.09 and 6.20 ± 0.51 $\mu\text{C cm}^{-2}$ for the KNN- CaTiO_3 film. A complete list of remnant polarization (P_r), maximum polarization (P_{max}) and coercive field (E_c) from Figure 4 and 5 is given in Table S.2 in the ESI.

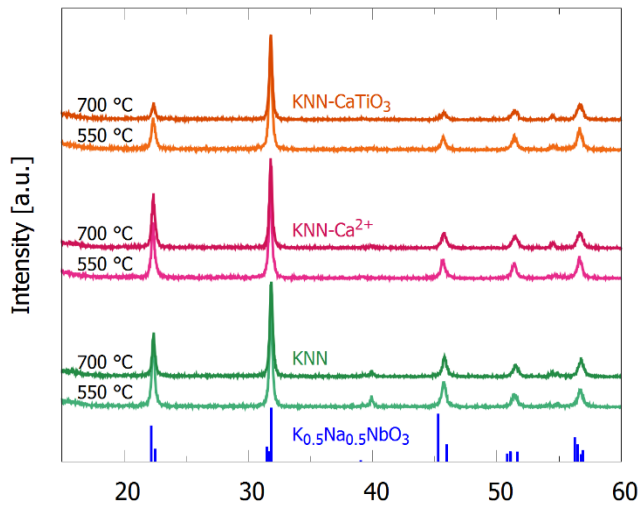


Figure 3: GIXRD patterns of pyrolyzed (550 °C) and annealed (700 °C) KNN films on SiPt. Reference pattern for $\text{K}_{0.5}\text{Na}_{0.5}\text{NbO}_3$ (blue, PDF card 00-061-0315⁷³) is included. The films were prepared by 30 repeating spin coatings.

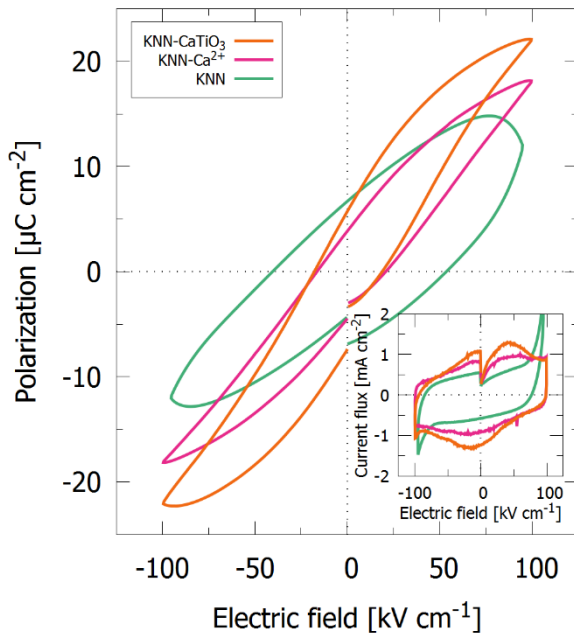


Figure 4: Polarization as a function of electric field for the KNN films. Ferroelectric polarization switching is observed for the doped films. The current fluxes during the measurements are included in the figure. A frequency of 10 Hz and an electric field bias of 100 kV cm^{-1} was used.

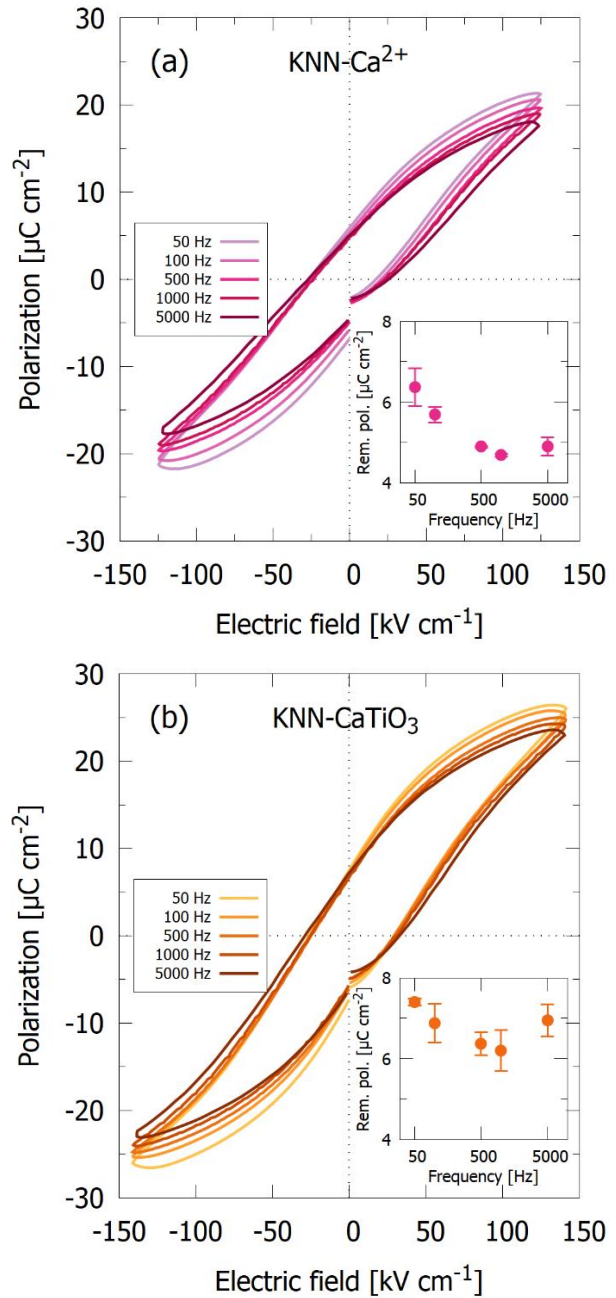


Figure 5: Polarization as a function of electric field measured at different frequencies for (a) Ca^{2+} -doped and (b) CaTiO_3 -doped KNN films. The measured remnant polarization plotted against frequency is provided as insets. Electric field biases of 125 kV cm^{-1} (KNN- Ca^{2+}) and 142 kV cm^{-1} (KNN- CaTiO_3) were used for the measurements.

The capacitances of the films as a function of electric field, displayed in Figure 6, were measured using an electric (DC) field of 100 kV cm^{-1} , a frequency of 500 Hz and an AC amplitude of 50 mV. The highest overall capacitance is observed in the film doped with CaTiO_3 , followed by the film doped with Ca^{2+} . Capacitance peaks at the coercive fields are modest and most predominant in the CaTiO_3 -doped film. The dielectric loss tangent ($\tan \delta$) for the measurement is included in the insert of Figure 6, demonstrating low losses in all the three films.

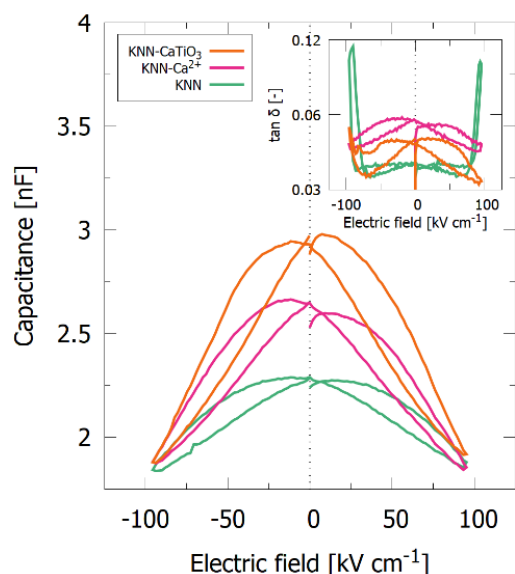


Figure 6: Capacitance as a function of electric field for the KNN films. The loss tangent is included as inset. An electric field of 100 kV cm⁻¹, a frequency of 500 Hz and an AC amplitude of 50 mV was used for the measurements.

The dielectric permittivity (ϵ') of the films as a function of temperature from 150 to 420 °C is presented in Figure 7. The data are shown for 1 kHz and an AC amplitude of 50 mV. A shallow maximum around ~210 °C and more pronounced maximum at 375 °C were observed for all the three compositions. The temperature at the maxima is not significantly shifted by doping KNN, indicating no major shift in the phase transition temperatures of KNN by the minor doping used in this study. Reproducible data below 150 °C could not be

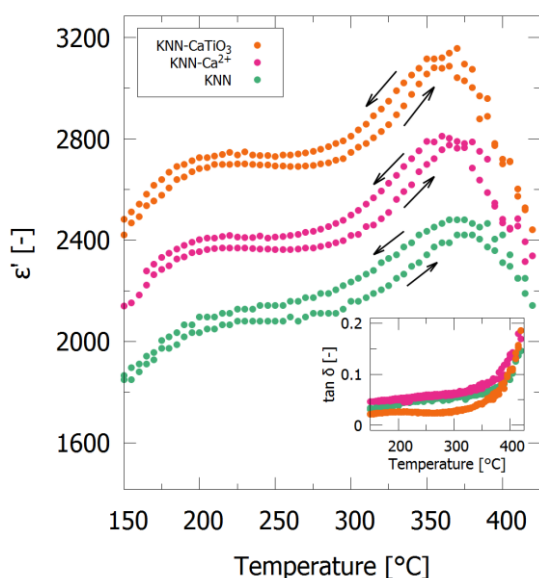


Figure 7: Real part of the dielectric permittivity at 1 kHz as a function of temperature of the three KNN films. Arrows indicate heating/cooling. Inset: The loss tangent measured at the same frequency. An AC amplitude of 50 mV was used in the measurements.

obtained are therefore not shown. Frequency dependency of the permittivity at 150 °C is plotted in Figure S.4 in the ESI.

Discussion

This study has demonstrated that both undoped and doped KNN films can be fabricated on SiPt substrates by aqueous CSD. The KNN films were homogenous, dense and phase pure as demonstrated by the scanning electron micrographs (Figure 2) and the GIXRD patterns (Figure 3). This is in line with our previous work on KNN films using (100) oriented SrTiO₃ (STO) single crystal substrates⁵⁶ and demonstrates that the aqueous precursor solution developed is suitable for fabricating high-quality KNN films on several types of substrates. Moreover, it was demonstrated that the aqueous precursor solution can be chemically modified to allow for compositional engineering of the KNN films. In this work complexes of Ca²⁺ and Ti⁴⁺ dissolved in water were used as dopants, but further doping with alkaline earth and rare earth elements should be possible. We have shown previously that aqueous precursor solutions can be applied to fabricate thin films of a whole range of different functional materials ranging from ferroelectric^{74,75}, transparent conducting^{76,77} and optical active materials⁷⁸.

Based on their ionic radii⁷⁹ and charge, Ca²⁺ and Ti⁴⁺ are proposed to be incorporated in the KNN lattice on the A- and B-site, respectively. Incorporation of the dopants in the KNN perovskite lattice was confirmed since no additional reflections in the diffraction patterns were observed for the powders from the precursor solutions (Figure 1) or the thin films (Figure 3 and Figure S.2). A decrease in the *c* lattice parameter and the unit cell volume, and an increase in the monoclinic β -distortion of the unit cell, were also observed in the doped KNN powders (Figure S.1/Table S.1), supporting the formation of solid solutions. The decrease in unit cell volume is expected due to the smaller sizes of the dopant cations compared to the inherent cations of KNN. The increase in crystallite size was much more prominent for the undoped KNN powder after heat treatment at 850 °C (Figure 1), suggesting that the doping strongly influences the mobility of the cations and reduces the grain growth in the doped KNN thin films (Figure 2). Suppressed grain growth has been observed in bulk samples doped with Ca²⁺ and CaTiO₃⁶⁶, and in thin films doped with CaZrO₃²⁹ and SrTiO₃⁴⁶. The coarsening is also influenced by the alkali excess, which has been shown to strongly promote grain growth in KNN⁸⁰. The alkali excess cannot however explain the difference in grain growth observed for the two doped materials since all three solutions used contained a considerable alkali excess.

The XRD patterns (Figure 3 and S.3) demonstrated that the KNN films were polycrystalline in nature with no preferential orientation or crystallographic texture. Textured films can possibly be obtained by tuning the processing conditions. We have previously reported on KNN films with (100) texture using (100) oriented single crystal STO substrates and the same precursor solution as used in this work⁵⁶. Promoting texture in KNN films on SiPt substrates has also been reported for both 2-

methoxyethanol- and water-based CSD syntheses by tuning the processing temperature or atmosphere^{34,57}.

Ferroelectric switching was clearly observed for the doped KNN films (Figure 4). A ferroelectric response was not observed for the undoped KNN film at any electric fields or frequencies, which is in line with our previous work using the same precursor solution, where only a weak ferroelectric response was obtained for undoped KNN films on STO substrates⁵⁶. Moreover, the hysteresis loops were also conducted at higher electric fields without breakdown for the CaTiO₃-doped films compared to the Ca²⁺-doped films, resulting in higher remnant polarizations for these two compositions (Figure 5). The maximum remnant polarization measured for the KNN-CaTiO₃ film (7.40±0.09 μC cm⁻²) is comparable with previous reports on KNN thin films^{19,23,25,29,36,40,47,48}.

Doping increases the capacitance of the KNN films by ~14.3% (Ca²⁺-doping) and ~29.1% (CaTiO₃-doping) at zero DC field, according to the data presented in Figure 6. This is in accordance with the permittivity shown in Figure 7, where the increases in permittivity were 15.4% (Ca²⁺-doping) and 32.0% (CaTiO₃-doping) at 150 °C. The values of the dielectric permittivity of the films as a function of temperature (Figure 7) are among the highest reported for KNN films from CSD^{20,21,26–28,30,31,33,34,36,42,46,47,51,53,54}. The dielectric loss of the three films (insets in Figure 6 and 7) showed only minor variations and were low for all three compositions.

0.5% doping with Ca²⁺ and CaTiO₃ only induced minor changes in the leakage current (inset Figure 4). The round-shaped P-E loop measured for undoped KNN (Figure 4) is a strong indication of high leakage currents, however the leakage was initiated at around 70 kV cm⁻¹, which is well above the coercive field of KNN. This demonstrates that the absence of ferroelectric switching is not due to low resistivity of the undoped KNN film. Hagh et al.⁸¹ reported an increase in resistivity by doping with 0.5-1.5 mol% Ba²⁺ in bulk KNN, implying that Ba²⁺ acts as a donor dopant in KNN. A similar effect might be expected for doping with other alkali earth metals, such as Ca²⁺, but this was not observed in the present work or in literature on bulk KNN^{63–65}.

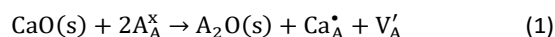
Only negligible changes due to doping were observed for the phase transitions induced from the permittivity (Figure 7). CaTiO₃-doping has been reported to decrease and diffuse/blur out the onset temperatures for the monoclinic to tetragonal (T_{M-T}) and tetragonal to cubic (T_C) phase transitions in bulk KNN and thereby improve ferroelectric polarization^{67–71}. This was not observed in this work as evident from the permittivity measurements shown in Figure 7.

Despite a low doping concentration (0.5 mol%), a significant effect was observed in the ferroelectric response. The origin is suggested to be related to the dopants' influence on the concentration of point defects in the crystal lattice although a difference in the dielectric loss could not be correlated with the doping. Charged defects like oxygen vacancies are associated

with domain wall pinning and dampening of the ferroelectric properties^{82,83}, and doping may influence on the concentration of oxygen vacancies. For co-doping with Ca²⁺/Ti⁴⁺ (CaTiO₃-doping), this can possibly be explained in terms of increased energy of formation for lattice defects, as defects like oxygen vacancies have a higher energy of formation in CaTiO₃ than in KNbO₃^{84,85}. For Ca²⁺-doping, a reduction in defect concentration can be explained in terms of charge compensation. As mentioned above, Ca²⁺ cations enter on the A-site in KNN. We propose three possible point defect equilibria for the incorporation of Ca²⁺, leading to A-site deficiency (A<B), stoichiometric A:B ratio (A=B) or A-site excess (A>B) in ABO₃. In all cases Ca²⁺ on the A-site, Ca_A[•], will have a formal charge of +1, which needs to be charge compensated.

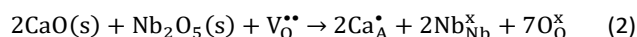
1) A<B, (K,Na)_{1-2x}Ca_xNbO₃:

When incorporated into the lattice, Ca²⁺ can form A-site deficiency according to Equation 1. Here the Ca²⁺ is charge compensated by the formation of an A-site vacancy, changing the A:B stoichiometry corresponding to (K,Na)_{1-2x}Ca_xNbO₃, as proposed by Malic et al.⁶⁵.



2) A=B, (K,Na)_{1-x}Ca_xNbO_{3+x/2}:

Alternatively, Ca²⁺ can be incorporated in KNN according to Equation 2, where Ca²⁺ is charge compensated by removal of oxygen vacancies in the lattice. In this case, the A:B stoichiometry is maintained (A:B = 1:1).



3) A>B, (K,Na)Ca_xNbO_{3+x}:

The third possibility involves charge compensation by removal of both an A-site vacancy and an oxygen vacancy as shown in Equation 3. This will form an excess on A-site (A>B) corresponding to (K,Na)Ca_xNbO_{3+x}.



During electrical characterization, no effect from Ca²⁺-doping was observed for the current flux (Figure 4) or the dielectric losses (insets in Figure 6 and 7), compared to undoped and CaTiO₃-doped KNN. This suggests that the overall concentration of mobile point defects like electron holes (h^{*}) is not affected by Ca²⁺-doping, and that the minor variations in the dielectric losses cannot be explained by the defect equilibria presented here. However, the ferroelectric properties (Figure 4) are improved with Ca²⁺-doping, and one explanation for this could be elimination of charged defects like oxygen and alkali vacancies, V_O^{••} and V'_A. As mentioned, such defects can pin ferroelectric domain walls and thereby reduce the ferroelectric response^{82,83}. In Equation 1, an alkali vacancy is formed, while in Equation 2 and 3 an oxygen vacancy is removed, suggesting that the latter mechanisms could reduce domain wall pinning. The number of A-site and oxygen vacancies increases at elevated temperatures due to increased evaporation of alkali

metals⁸⁶, which means that Equation 1 is most relevant for high-temperature processing of KNN. For low-temperature processing of KNN, or when using high amounts of excess alkali metals, Equation 2 and 3 are more likely. In this work, a low processing temperature (700 °C, 10 min) and an alkali excess (5 mol% Na⁺ and K⁺) was used, making Equation 2 and 3 the most plausible point defect equilibria for Ca²⁺ incorporation. Following this, Ca²⁺-doping is proposed to have a positive influence on reduction of domain wall pinning in KNN, as reflected in the improved ferroelectric properties presented in this work (Figure 4 and 5).

Conclusions

Phase pure KNN thin films with three different compositions (undoped KNN, 0.5 mol% Ca²⁺-doped KNN, 0.5 mol% Ca²⁺/Ti⁴⁺ co-doped KNN) were successfully fabricated on platinized silicon substrates by aqueous CSD. Reduced grain growth was observed in the doped films and powders prepared from the precursor solutions, suggesting that the dopants reduce cation mobility. A reduction in unit cell volume was observed in the doped KNN powders. The effect of 0.5 mol% Ca²⁺-doping and 0.5 mol% Ca²⁺-Ti⁴⁺ co-doping on the ferroelectric and dielectric properties of the KNN films was measured using Pt top electrodes. Polarization switching was observed in the doped KNN films in the frequency range 10 to 5000 Hz, with peak remnant polarization of 6.37±0.47 and 7.40±0.09 μC cm⁻² for Ca²⁺- and CaTiO₃-doping, respectively. Polarization switching was not observed in the undoped KNN films. All films had exceptionally high dielectric constants, ranging from 1800 to 3200, measured at 1 kHz in the temperature range 150 to 420 °C. The capacitance of the doped films was ~15% (Ca²⁺-doping) and ~30% (CaTiO₃-doping) higher than the undoped KNN films. No significant difference in leakage currents or phase transition temperatures was observed between the films. The improved ferroelectric properties from doping is suggested to be linked to reduced defect concentration due to higher energies of formation (CaTiO₃-doping) or shifted defect equilibrium (Ca²⁺-doping).

Conflicts of interest

There are no conflicts to declare.

Acknowledgements

Financial support from the Research Council of Norway through NANO2021 project PIEZOMED project number 250184 is acknowledged. Dr. Magnus Rotan is acknowledged for the support regarding X-ray diffractogram fitting using the Pawley method.

References

1. Wu J, Xiao D, Zhu J. Potassium–Sodium Niobate Lead-Free Piezoelectric Materials: Past, Present, and Future of Phase Boundaries. *Chem Rev.* 2015;115:2559–95.
2. Rödel J, Webber KG, Dittmer R, Jo W, Kimura M, Damjanovic D. Transferring lead-free piezoelectric ceramics into application. *J Eur Ceram Soc.* 2015;35(6):1659–81.
3. Manjón-sanz AM, Dolgos MR. Applications of Piezoelectrics: Old and New. *Chem Mater.* 2018;30(24):8718–26.
4. Zhang Y, Li JF. Review of chemical modification on potassium sodium niobate lead-free piezoelectrics. *J Mater Chem C.* 2019;7(15):4284–303.
5. Joung Y-H. Development of Implantable Medical Devices: From an Engineering Perspective. *Int Neurourol J.* 2013;17:98–106.
6. Yu S-W, Kuo S-T, Tuan W-H, Tsai Y-Y, Su C-H. Ion release from three lead-free piezoelectric ceramics and their physical and cytotoxicity characteristics. *Mater Lett.* 2011 Dec;65(23–24):3522–4.
7. Yu S, Kuo S, Tuan W, Tsai Y, Wang S. Cytotoxicity and degradation behavior of potassium sodium niobate piezoelectric ceramics. *Ceram Int.* 2012;38(4):2845–50.
8. Chen W, Yu Z, Pang J, Yu P, Tan G, Ning C. Fabrication of Biocompatible Potassium Sodium Niobate Piezoelectric Ceramic as an Electroactive Implant. *Materials (Basel).* 2017;10:345.
9. Yao T, Chen J, Wang Z, Zhai J, Li Y, Xing J, et al. The antibacterial effect of potassium-sodium niobate ceramics based on controlling piezoelectric properties. *Colloids Surfaces B Biointerfaces.* 2018;175:463–8.
10. Jeong CK, Han JH, Palneedi H, Park H, Hwang G, Joung B, et al. Comprehensive biocompatibility of nontoxic and high-output flexible energy harvester using lead-free piezoceramic thin film. *Appl Mater.* 2017;5:74102.
11. Wang Q, Yang J, Zhang W, Khoie R, Li YM, Zhu JG, et al. Manufacture and cytotoxicity of a lead-free piezoelectric ceramic as a bone substitute-consolidation of porous lithium sodium potassium niobate by cold isostatic pressing. *Int J Oral Sci.* 2009;1(2):99–104.
12. Kim BY, Lee WH, Hwang HG, Kim DH, Kim JH, Lee SH, et al. Resistive Switching Memory Integrated with Nanogenerator for Self-Powered Bioimplantable Devices. *Adv Funct Mater.* 2016;26(29):5211–21.
13. Tan G, Wang S, Zhu Y, Zhou L, Yu P, Wang X, et al. Surface-Selective Preferential Production of Reactive Oxygen Species on Piezoelectric Ceramics for Bacterial Killing. *ACS Appl Mater Interfaces.* 2016;8(37):24306–9.
14. Seog HJ, Lee SY, Park J. Recent Progress in Potassium Sodium Niobate Lead-free Thin Films. *J Korean Phys Soc.* 2018;72(12):1467–83.
15. Zhang SW, Zhou Z, Luo J, Li JF. Potassium-Sodium-Niobate-Based Thin Films: Lead Free for Micro-Piezoelectrics. *Ann Phys.* 2019;531(7):1800525.
16. Thong HC, Zhao C, Zhou Z, Wu CF, Liu YX, Du ZZ, et al. Technology transfer of lead-free (K, Na)NbO₃-based piezoelectric ceramics. *Mater Today.* 2019;29:37–48.
17. Bassiri-Gharb N, Bastani Y, Bernal A. Chemical solution growth of ferroelectric oxide thin films and nanostructures. *Chem Soc Rev.* 2014;43:2125–40.
18. Yu Q, Li J-F, Sun W, Zhou Z, Xu Y, Xie Z-K, et al. Electrical properties of K_{0.5}Na_{0.5}NbO₃ thin films grown on Nb:SrTiO₃ single-crystalline substrates with different crystallographic orientations. *J Appl Phys.* 2013;113:24101.

19. Kondo N, Sakamoto W, Lee B, Iijima T, Kumagai J, Moriya M, et al. Improvement in Ferroelectric Properties of Chemically Synthesized Lead-Free Piezoelectric (K,Na)(Nb,Ta)O₃ Thin Films by Mn Doping. *Jpn J Appl Phys.* 2010;49:09MA04.
20. Ahn CW, Seog HJ, Ullah A, Lee SY, Kim JW, Kim SS, et al. Effect of Ta content on the phase transition and piezoelectric properties of lead-free (K_{0.48}Na_{0.48}Li_{0.04})(Nb_{0.995-x}Mn_{0.005}Ta_x)O₃ thin film. *J Appl Phys.* 2012;111:24110.
21. Lee SY, Ahn CW, Kim JS, Ullah A, Lee HJ, Hwang H-I, et al. Enhanced piezoelectric properties of Ta substituted-(K_{0.5}Na_{0.5})NbO₃ films: A candidate for lead-free piezoelectric thin films. *J Alloys Compd.* 2011;509(20):L194–8.
22. Lai F, Li J-F, Zhu Z-X, Xu Y. Influence of Li content on electrical properties of highly piezoelectric (Li,K,Na)NbO₃ thin films prepared by sol-gel processing. *J Appl Phys.* 2009;106(6):64101.
23. Nakashima Y, Sakamoto W, Maiwa H, Shimura T, Yogo T. Lead-Free Piezoelectric (K,Na)NbO₃ Thin Films Derived from Metal Alkoxide Precursors. *Japan Soc Appl Phys.* 2007;46(14):L311–3.
24. Wang Y, Yao K, Mirshekarloo MS, Eng F, Tay H. Effects and Mechanism of Combinational Chemical Agents on Solution-Derived K_{0.5}Na_{0.5}NbO₃ Piezoelectric Thin Films. *J Am Ceram Soc.* 2016;99(5):1631–6.
25. Yu Q, Li J, Chen Y, Cheng L, Sun W, Zhou Z, et al. Effect of Pyrolysis Temperature on Sol – Gel Synthesis of Lead-free Piezoelectric (K,Na)NbO₃ Films on Nb:SrTiO₃ Substrates. *J Am Ceram Soc.* 2014;97:107–13.
26. Vendrell X, Raymond O, Ochoa DA, Garcia JE, Mestres L. Growth and physical properties of highly oriented La-doped (K,Na)NbO₃ ferroelectric thin films. *Thin Solid Films.* 2015;577:35–41.
27. Luo J, Sun W, Zhou Z, Bai Y, Wang ZJ, Tian G, et al. Domain Evolution and Piezoelectric Response across Thermotropic Phase Boundary in (K,Na)NbO₃-Based Epitaxial Thin Films. *Appl Mater Interfaces.* 2017;9:13315–22.
28. Zhang X, Liu J, Zhu K, Wang J, Li Z. Effects of Mn doping on dielectric and ferroelectric characteristics of lead-free (K,Na,Li)NbO₃ thin films grown by chemical solution deposition. *J Mater Sci Mater Electron.* 2017;28(1):487–92.
29. Matsuda T, Sakamoto W, Takashi BL, Jun I, Makoto K, Toshiobu M. Electrical Properties of Lead-Free Ferroelectric Mn-Doped K_{0.5}Na_{0.5}NbO₃-CaZrO₃ Thin Films Prepared by Chemical Solution Deposition. *Jpn J Appl Phys.* 2012;51:09LA03.
30. Lee SY, Ahn CW, Ullah A, Seog HJ, Kim JS, Bae SH, et al. Effect of Mn substitution on ferroelectric and leakage current characteristics of lead-free (K_{0.5}Na_{0.5})(Mn_xNb_{1-x})O₃ thin films. *Curr Appl Phys.* 2011;11(3):S266–9.
31. Goh PC, Yao K, Chen Z. Lithium diffusion in (Li,K,Na)NbO₃ piezoelectric thin films and the resulting approach for enhanced performance properties. *Appl Phys Lett.* 2011;99:92902.
32. Ahn CW, Jeong ED, Lee SY, Lee HJ, Kang SH, Kim IW. Enhanced ferroelectric properties of LiNbO₃ substituted Na_{0.5}K_{0.5}NbO₃ thin films grown by chemical solution deposition. *Appl Phys Lett.* 2008;93:212905.
33. Wang L, Zuo R, Liu L, Su H, Shi M, Chu X, et al. Preparation and characterization of sol-gel derived (Li,Ta,Sb) modified (K,Na)NbO₃ lead-free ferroelectric thin films. *Mater Chem Phys.* 2011;130(1–2):165–9.
34. Zhang SW, Luo J, Zhou Z, Li JF. Sol-gel processed highly (100)-textured (K, Na)NbO₃-based lead-free thin films: Effect of pyrolysis temperature. *J Am Ceram Soc.* 2019;102(5):2696–705.
35. Wang L, Ren W, Shi P, Wu X. Cobalt doping effects on structures and electrical properties of lead-free ferroelectric K_{0.5}Na_{0.5}NbO₃ films. *J Alloys Compd.* 2014;608:202–6.
36. Wang L, Ren W, Goh PC, Yao K, Shi P, Wu X, et al. Structures and electrical properties of Mn- and Co-doped lead-free ferroelectric K_{0.5}Na_{0.5}NbO₃ films prepared by a chemical solution deposition method. *Thin Solid Films.* 2013;537:65–9.
37. Luo J, Zhang S, Zhou Z, Zhang Y, Lee HY, Yue Z, et al. Phase transition and piezoelectricity of BaZrO₃-modified (K,Na)NbO₃ lead-free piezoelectric thin films. *J Am Ceram Soc.* 2019;102(5):2770–80.
38. Tanaka K, Kakimoto K, Ohsato H. Fabrication of highly oriented lead-free (Na, K)NbO₃ thin films at low temperature by Sol-Gel process. *J Cryst Growth.* 2006;294(2):209–13.
39. Nakashima Y, Sakamoto W, Yogo T. Processing of highly oriented (K,Na)NbO₃ thin films using a tailored metal-alkoxide precursor solution. *J Eur Ceram Soc.* 2011;31(14):2497–503.
40. Kupec A, Malic B, Tellier J, Tchernychova E, Glinsek S, Kosec M. Lead-Free Ferroelectric Potassium Sodium Niobate Thin Films from Solution: Composition and Structure. *J Am Ceram Soc.* 2012;95(2):515–23.
41. Kupec A, Uršič H, Frunzä RC, Tchernychova E, Malič B. Microstructure-dependent leakage-current properties of solution-derived (K_{0.5}Na_{0.5})NbO₃ thin films. *J Eur Ceram Soc.* 2015;35(13):3507–11.
42. Lee SY, Seog HJ, Ahn CW, Ullah A, Kim IW. Interfacial Dead Layers on Lead Free Ferroelectric (K_{0.5}Na_{0.5})(Mn_{0.005}Nb_{0.995})O₃ Thin Films. *Jpn J Appl Phys.* 2012;51:09MD03.
43. Zhao C, Meng X, Wang W, Zhou Y. Energy storage performance of (K, Na)NbO₃ ferroelectric thin films with Mn-Ta and Mn-Ti co-doping. *Ceram Int.* 2019;45(11):13772–9.
44. Lai F, Li JF. Sol-gel processing and characterization of (Na,K)NbO₃ lead-free ferroelectric films. *Ferroelectrics.* 2007;358:181–7.
45. Lai F, Li JF. Sol-gel processing of lead-free (Na,K)NbO₃ ferroelectric films. *J Sol-Gel Sci Technol.* 2007;42(3):287–92.
46. Kupec A, Malič B. Structural and dielectric properties of the lead-free (1-x)K_{0.5}Na_{0.5}NbO₃-xSrTiO₃ thin films from solutions. *J Alloys Compd.* 2014;596:32–8.
47. Lee SY, Kim JS, Ahn CW, In Hwang H, Kim W. Impedance spectroscopy and relaxation phenomena of (Na,K) excess Na_{0.5}K_{0.5}NbO₃ thin films grown by chemical solution deposition. *Thin Solid Films.* 2010;519(2):947–51.
48. Wang L, Ren W, Shi P, Chen X, Wu X, Yao X. Enhanced ferroelectric properties in Mn-doped K_{0.5}Na_{0.5}NbO₃ thin films derived from chemical solution deposition. *Appl Phys Lett.* 2010;97(7):72902.
49. Tkach A, Santos A, Zlotnik S, Serrazina R, Okhay O, Bdikin I, et al. Effect of solution conditions on the properties of sol-gel derived potassium sodium niobate thin films on platinumized sapphire substrates. *Nanomaterials.* 2019;9(11):1600.
50. Grivel J, Thydén K, Bowen JR, Haugen AB. Deposition of highly oriented (K,Na)NbO₃ films on flexible metal substrates. *Thin Solid Films.* 2018;650(December 2017):7–10.

51. Kwak J, Kingon AI, Kim SH. Lead-free (Na_{0.5},K_{0.5})NbO₃ thin films for the implantable piezoelectric medical sensor applications. *Mater Lett.* 2012;82:130–2.
52. Lu T, Zhu K, Liu J, Wang J, Qiu J. Lead-free (K,Na)NbO₃ thin films derived from chemical solution deposition modified with EDTA. *J Mater Sci.* 2014;25:1112–6.
53. Zhang D, Zheng F, Yang X, Liu H, Cao M. Preparation and ferroelectric properties of K_{0.5}Na_{0.5}NbO₃ thin films derived from non-alcohol niobium salt sol-gel process. *Integr Ferroelectr.* 2014;4587(September 2016):673–8.
54. Yao L, Zhu K, Wang J, Liu J, Qiu J, Cheng M, et al. Annealing temperature effects on the electrical properties of (K,Na)NbO₃ thin film fabricated by a sol-gel process with a citrate precursor solution. *Ferroelectrics.* 2016;493:47–53.
55. Pham K, Gaukås NH, Morozov M, Tybell T, Vullum PE, Grande T, et al. Epitaxial K_{0.5}Na_{0.5}NbO₃ thin films by aqueous chemical solution deposition. *R Soc Open Sci.* 2019;6:180989.
56. Gaukås NH, Dale SM, Ræder TM, Toresen A, Holmestad R, Glaum J, et al. Controlling phase purity and texture of K_{0.5}Na_{0.5}NbO₃ thin films by aqueous chemical solution deposition. *Materials (Basel).* 2019;12:2042.
57. Zhang W, Zhu H, Zhang X, Wu H, Bao J, Hu F. Structural and electrical study of highly (100)-oriented KNN films fabricated by a sol-gel non-alkoxide process. *Ceram Int.* 2019;14(17):22156–62.
58. Bruncková H, Medvecký L, Hvizdoš P. Effect of substrate on microstructure and mechanical properties of sol-gel prepared (K, Na)NbO₃ thin films. *Mater Sci Eng B Solid-State Mater Adv Technol.* 2013;178(4):254–62.
59. Bruncková H, Medvecký L, Hvizdoš P, Ďurišin J. Structural and nanomechanical properties of sol-gel prepared (K, Na)NbO₃ thin films. *Surf Interface Anal.* 2015;47(11):1063–71.
60. Rödel J, Jo W, Seifert KTP, Anton EM, Granzow T, Damjanovic D. Perspective on the development of lead-free piezoceramics. *J Am Ceram Soc.* 2009;92(6):1153–77.
61. Puleo DA, Huh WW. Acute toxicity of metal ions in cultures of osteogenic cells derived from bone marrow stromal cells. *J Appl Biomater.* 1995;6(2):109–16.
62. Fraga CG. Relevance, essentiality and toxicity of trace elements in human health. *Mol Aspects Med.* 2005;26(4–5):235–44.
63. Taub J, Ramajo L, Castro MS. Phase structure and piezoelectric properties of Ca- and Ba-doped K_{0.5}Na_{0.5}NbO₃ lead-free ceramics. *Ceram Int.* 2013;39(4):3555–61.
64. Tang L, Liu T, Ma J, Zhang X, An L, Chen K. Ca²⁺ doping effects in (K, Na, Li)(Nb_{0.8}Ta_{0.2})O₃ lead-free piezoelectric ceramics. *Front Mater Sci.* 2019;13:431–8.
65. Malic B, Bernard J, Holc J, Jenko D, Kosec M. Alkaline-earth doping in (K,Na)NbO₃ based piezoceramics. *J Eur Ceram Soc.* 2005;25:2707–11.
66. Zhuk M, Einarsrud MA, Glaum J. in preparation.
67. Park H, Cho K, Paik D, Nahm S, Lee H, Kim D. Microstructure and piezoelectric properties of lead-free (1-x)(Na_{0.5}K_{0.5})NbO₃-xCaTiO₃ ceramics. *J Appl Phys.* 2007;102:124101.
68. Ramajo L, Parra R, Castro MS. Electrical and microstructural properties of CaTiO₃-doped K_{0.5}Na_{0.5}NbO₃-lead free ceramics. *Bull Mater Sci.* 2011;34(6):1213–7.
69. Wu J, Xiao D, Wang Y, Wu W, Zhang B, Zhu J. Improved temperature stability of CaTiO₃-modified [(K_{0.5}Na_{0.5})_{0.96}Li_{0.04}](Nb_{0.91}Sb_{0.05}Ta_{0.04})O₃ lead-free piezoelectric ceramics. *J Appl Phys.* 2008;104:24102.
70. Chang Y, Yang Z, Chao X, Zhang R, Li X. Dielectric and piezoelectric properties of alkaline-earth titanate doped (K_{0.5}Na_{0.5})NbO₃ ceramics. *Mater. Lett.* 2007;61:785–9.
71. Chen H, Liu P. Electrical properties of 0.98(K_{0.5}Na_{0.5})NbO₃-0.02AETiO₃ piezoceramics doped with Li₂CO₃. *Ferroelectrics.* 2019;551(1):53–9.
72. Ikeuchi S, Yoneda T, Matsuki Y, Endo N, Takeshima Y, Horiuchi H, et al. Preparation of (K,Na)NbO₃-CaTiO₃ film by RF magnetron sputtering. In: 2014 IEEE International Ultrasonics Symposium Proceedings. IEEE; 2014. p. 1578–81.
73. Tellier J, Malic B, Dkhil B, Jenko D, Cilensek J, Kosec M. Crystal structure and phase transitions of sodium potassium niobate perovskites. *Solid State Sci.* 2009;11(2):320–4.
74. Christensen M, Einarsrud MA, Grande T. Fabrication of lead-free Bi_{0.5}Na_{0.5}TiO₃ thin films by aqueous chemical solution deposition. *Materials (Basel).* 2017;10(2):213.
75. Raeder TM, Bakken K, Glaum J, Einarsrud MA, Grande T. Enhanced in-plane ferroelectricity in BaTiO₃ thin films fabricated by aqueous chemical solution deposition. *AIP Adv.* 2018;8(10):105228.
76. Sunde TOL, Garskaite E, Otter B, Fossheim HE, Sæterli R, Holmestad R, et al. Transparent and conducting ITO thin films by spin coating of an aqueous precursor solution. *J Mater Chem.* 2012;22(31):15740.
77. Sunde TOL, Einarsrud MA, Grande T. Optimisation of chemical solution deposition of indium tin oxide thin films. *Thin Solid Films.* 2014;573(3):48–55.
78. Garskaite E, Lindgren M, Einarsrud MA, Grande T. Luminescent properties of rare earth (Er, Yb) doped yttrium aluminium garnet thin films and bulk samples synthesised by an aqueous sol-gel technique. *J Eur Ceram Soc.* 2010;30(7):1707–15.
79. Shannon RD. Revised Effective Ionic Radii and Systematic Studies of Interatomic Distances in Halides and Chalcogenides. *Acta Crystallogr Sect A Cryst physics, diffraction, Theor Gen Crystallogr.* 1976;32(5):751–67.
80. Bomlai P, Wichianrat P, Muensit S, Milne SJ. Effect of Calcination Conditions and Excess Alkali Carbonate on the Phase Formation and Particle Morphology of Na_{0.5}K_{0.5}NbO₃ Powders. *J Am Ceram Soc.* 2007;90(5):1650–5.
81. Hagh NM, Jadidian B, Ashbahian E, Safari A. Lead-Free piezoelectric ceramic transducer in the donor-doped K_{1/2}Na_{1/2}NbO₃ solid solution system. *IEEE Trans Ultrason Ferroelectr Freq Control.* 2008;55(1):214–24.
82. Bassiri-Gharb N, Fujii I, Hong E, Trolier-Mckinstry S, Taylor DV, Damjanovic D. Domain wall contributions to the properties of piezoelectric thin films. *J Electroceramics.* 2007;19(1):47–65.
83. Xu F, Trolier-Mckinstry S, Ren W, Xu B, Xie ZL, Hemker KJ. Domain wall motion and its contribution to the dielectric and piezoelectric properties of lead zirconate titanate films. *J Appl Phys.* 2001;89(2):1336–48.
84. Lee H, Mizoguchi T, Yamamoto T, Ikuhara Y. First principles study on intrinsic vacancies in cubic and orthorhombic CaTiO₃. *Mater Trans.* 2009;50(5):977–83.
85. Shigemi A, Wada T. Evaluations of phases and vacancy formation energies in KNbO₃ by first-principles calculation. *Japanese J Appl Physics, Part 1 Regul Pap Short Notes Rev Pap.* 2005;44(11):8048–54.
86. Popovič A, Bencze L, Koruza J, Malič B. Vapour pressure and mixing thermodynamic properties of the KNbO₃-NaNbO₃ system. *RSC Adv.* 2015;5(93):76249–56.

ARTICLE